Inorganic Chemistry

Article

pubs.acs.org/IC

Structure and Magnetic Properties of the Spin-1/2-Based Honeycomb $NaNi_2BiO_{6-\delta}$ and Its Hydrate $NaNi_2BiO_{6-\delta}\cdot 1.7H_2O$

Elizabeth M. Seibel,*[,†] John H. Roudebush,[†] Mazhar N. Ali,[†] K. A. Ross,[‡,§] and R. J. Cava*[,†]

[†]Department of Chemistry, Princeton University, Princeton, New Jersey 08544, United States

[‡]Institute for Quantum Matter and Department of Physics and Astronomy, Johns Hopkins University, Baltimore, Maryland 21218, United States

[§]NIST Center for Neutron Research, National Institute of Standards and Technology, Gaithersburg, Maryland 20899, United States

Supporting Information

ABSTRACT: We present the structure and magnetic properties of the honeycomb anhydrate $NaNi_2BiO_{6-\delta}$ and its monolayer hydrate $NaNi_2BiO_{6-\delta}\cdot 1.7H_2O$, synthesized by deintercalation of the layered α-$NaFeO_2$-type honeycomb compound $Na_3Ni_2BiO_6$. The anhydrate adopts ABAB-type oxygen packing and a one-layer hexagonal unit cell, whereas the hydrate adopts an oxygen packing sequence based on a three-layer rhombohedral subcell. The metal-oxide layer separations are 5.7 Å in the anhydrate and 7.1 Å in the hydrate, making the hydrate a quasi 2-D honeycomb system. The compounds were characterized through single crystal diffraction, powder X-ray diffraction, thermogravimetric analysis, and elemental analysis. Temperature-dependent magnetic susceptibility measurements show both to have negative Weiss temperatures (−18.5 and −14.6 K, respectively) and similar magnetic moments (2.21 and 2.26 μ_B/Ni, respectively), though the field-dependent magnetization and heat capacity data suggest subtle differences in their magnetic behavior. The magnetic moments per Ni are relatively high, which we suggest is due to the presence of a mixture of Ni^{2+} and Ni^{3+} caused by oxygen vacancies.

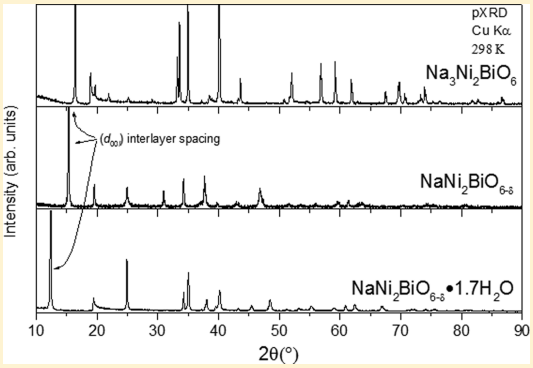

INTRODUCTION

Magnetic atoms on honeycomb lattices have garnered much attention due to the complex magnetism that they often display. Though not typically considered a magnetically frustrating geometry due to the possibility of simple Néel antiferromagnetic (AFM) ordering, frustration of that ordering on honeycombs can arise from interactions between nearest neighbor (NN) and next-nearest neighbor (NNN) spins.[1] Spin-1/2, layered honeycomb compounds, like Na_2IrO_3, are of particular interest due to the exotic properties that such systems are expected to exhibit.[2,3] Recently, the honeycomb compounds $Na_3Ni_2SbO_6$ and $Na_3Co_2SbO_6$ were deintercalated and subsequently hydrated to form $Na_{0.95}Ni_2SbO_6\cdot 1.5H_2O$ and $Na_{0.85}Co_2SbO_6\cdot 1.7H_2O$, respectively. These compounds display markedly different magnetism from their parent structures, and the Ni variant is an example of a spin-1/2, quasi 2-D honeycomb system.[4] Hydration causes a significant increase in layer spacing; the importance of this with respect to magnetic and electronic properties has been exemplified by the sodium cobalt oxyhydrate family where superconductivity in the bilayer hydrate (BLH) $Na_{0.3}CoO_2\cdot 1.4H_2O$ is absent in the monolayer hydrate (MLH) and the anhydrous compound.[5] The hydration of many layered magnetic oxides has since been explored to create low-dimensional systems.[6−10] We therefore set out to make a new, spin-1/2 honeycomb compound with well-separated metal-oxide layers.

We report here the synthesis, structure, and magnetic properties of the spin-1/2-based honeycomb anhydrate $NaNi_2BiO_{6-\delta}$ and its hydrate, $NaNi_2BiO_{6-\delta}\cdot 1.7H_2O$; the latter is structurally analogous to $Na_{0.95}Ni_2SbO_6\cdot 1.5H_2O$. The structure of the parent compound, $Na_3Ni_2BiO_6$, has been previously reported as an ordered, α-$NaFeO_2$-type honeycomb.[11] Briefly, this parent structure consists of layers of edge-shared Ni^{2+} and Bi^{5+} octahedra in a 2:1 ratio such that the ordering forms a honeycomb of spin-1 magnetic nickel ions. Here, we show that treatment of $Na_3Ni_2BiO_6$ with Br_2/ dry CH_3CN causes the removal of two Na^+ per formula unit and the oxidation of Ni^{2+} to Ni^{3+}. Exposure of the resulting anhydrate $NaNi_2BiO_{6-\delta}$ to ambient air results in the intercalation of water within the sodium layer, causing layer gliding, and further separating the metal-oxide layers to produce the hydrate $NaNi_2BiO_{6-\delta}\cdot 1.7H_2O$. We determine the formulas of the compounds through a combination of elemental analysis and thermogravimetric analysis (TGA). The magnetic properties of both compounds are presented and discussed in accordance with their structures. Importantly, the metal-oxide layer spacing increases from 5.7 to7.1 Å with hydration, creating a honeycomb with quasi 2-D character.

Received: June 17, 2014
Published: October 2, 2014

EXPERIMENTAL SECTION

Polycrystalline $Na_3Ni_2BiO_6$ was made as previously reported.[11] Approximately 1 g of the material was then allowed to stir in a 50 mL solution of 6 M Br_2/dry CH_3CN for 24 h at room temperature. The resulting black powder of $NaNi_2BiO_{6-\delta}$ was filtered, washed with dry CH_3CN, dried under nitrogen, and immediately moved to an argon-filled, dry glovebox to prevent water uptake. Exposure of the powder to humid laboratory air for 24 h produced the hydrate $NaNi_2BiO_{6-\delta}\cdot 1.7H_2O$. Both samples were characterized by powder X-ray diffraction (PXRD) using a Bruker D8 FOCUS diffractometer with Cu Kα radiation and a diffracted beam monochromator. Powder diffraction patterns were refined using the Full Prof Suite, with peak shapes refined using the Thomson-Cox-Hasting pseudo-Voigt function with the background set as a linear interpolation of fixed points.[12]

Single crystals of the anhydrate $NaNi_2BiO_{6-\delta}$ were obtained by treating the previously reported single crystals of $Na_3Ni_2BiO_6$,[11] approximately 2 × 3 × 0.2 mm, with 20 mL of 6 M Br_2/dry CH_3CN for 24 h at room temperature without stirring. The crystals changed from brown to black, consistent with the polycrystalline samples. The crystals were filtered, washed with dry CH_3CN, dried under nitrogen, and immediately moved to an argon-filled, dry glovebox. Hydrate crystals were made by soaking the anhydrate crystals in water overnight. The surfaces of both the anhydrate and hydrate single crystals were rough and irregular, and twinning was observed in all tested pieces. Single crystal X-ray diffraction (SXRD) was conducted on a Bruker APEX II diffractometer with Mo Kα radiation at 100 K. Unit cell refinement and data integration was performed with Bruker APEX II software[13] and CELL_NOW.[14] The crystal structures were refined using the full-matrix least-squares method on F^2, implemented through SHELXTL-2013[15] and WinGX.[16]

Elemental analysis of the polycrystalline hydrate sample was performed at Galbraith Laboratories, Knoxville, TN, using ICP-OES. To determine water content, TGA was performed on a TA Instruments SDT Q600 instrument by both allowing the anhydrate to gain mass under wet air and by heating the hydrate at 0.25 °C/min from room temperature to 300 K under flowing air. Reduction of $NaNi_2BiO_{6-\delta}$ under 10% H_2/90% Ar was performed from 25 to 550 °C at 0.5 °C/min to determine oxygen content.

A Quantum Design Physical Property Measurement System (PPMS) was used to collect temperature- and field-dependent magnetization data as well as heat capacity (HC). All magnetic measurements were performed on the polycrystalline materials. Zero field cooled (ZFC) magnetization data was taken from 2 to 300 K in an applied field of $\mu_0\mathbf{H}$ = 1 T, and susceptibility was defined as $M/\mathbf{H}$. Field-dependent magnetization measurements were taken at 2, 5, 10, and 30 K with a sweep from 0 to 9 T. HC measurements were conducted from 2 to 100 K in 0, 3, 6, and 9 T fields by mounting pressed pellets of the samples on a sapphire platform with Apiezon N grease.

RESULTS AND DISCUSSION

Structure. X-ray powder diffraction patterns of $NaNi_2BiO_{6-\delta}$, $NaNi_2BiO_{6-\delta}\cdot 1.7H_2O$, and the parent $Na_3Ni_2BiO_6$ are shown in Figure 1. The interlayer spacing along the c-direction increases with the removal of sodium from the decrease of Na−O Coulombic attraction in the layers and from increased electrostatic repulsion between layers caused by the oxidation of nickel, similar to what is observed for Na_xCoO_2.[17] Hydration then further separates these layers to a distance of ∼7.1 Å, consistent with the Sb-analogue and other MLHs.[4,6,18] As has been discussed previously,[11] the parent compound $Na_3Ni_2BiO_6$ can be indexed to an $R\bar{3}m$ subcell, which means the oxygen packing sequence creates a three-layer-derived structure. In such a structure, all metal oxide octahedra face the same direction and sodium is octahedrally coordinated between the layers. The parent is actually a 1-layer monoclinic cell, like many other honeycomb compounds,[19−24] with O1-type

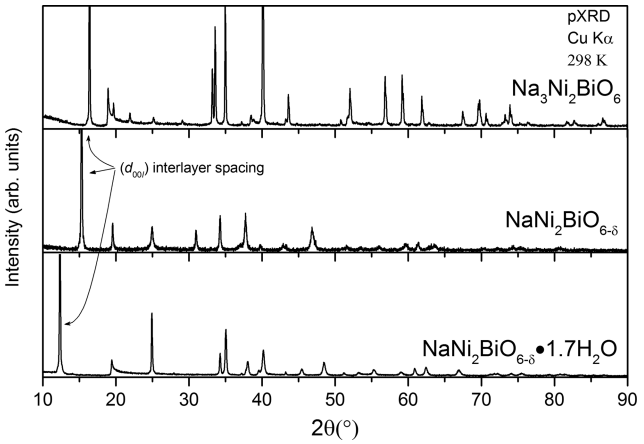

Figure 1. Room-temperature PXRD data of $Na_3Ni_2BiO_6$ (top), $NaNi_2BiO_{6-\delta}$ (middle), and $NaNi_2BiO_{6-\delta}\cdot 1.7H_2O$ (bottom). The expansion in the metal-oxide layer spacing(d_{00l}) upon sodium removal and hydration is highlighted.

stacking.[11] However, the anhydrate $NaNi_2BiO_{6-\delta}$ is indexed to a hexagonal cell rather than a rhombohedral cell, indicating that the oxygen packing sequence changes. As has been discussed previously, low-temperature ionic exchange reactions cannot cause octahedral rotation as this would require the breaking of metal-oxide bonds; only metal-oxide slab translation is allowed.[25,26] Stacking rearrangements caused by such translations were studied in detail for the deintercalation of Na_xCoO_2.[17] O3−P3 and O2−P2 phase transitions have also been extensively studied during electrochemical cycling of ABO_2 layered materials as positive electrodes (A = alkali, B = transition metal); again, at no time does metal-oxide bond breaking occur.[27] Therefore, $NaNi_2BiO_{6-\delta}$ must adopt a new oxygen packing sequence compared to $Na_3Ni_2BiO_6$ by sliding of the metal oxide slabs, and all octahedra must still face the same direction. Water intercalation then causes layer shifting back to an $R\bar{3}m$ subcell, which suggests a 3-layer-derived structure for the hydrate $NaNi_2BiO_{6-\delta}\cdot 1.7H_2O$. The structural refinements are discussed below.

The composition of the hydrate was found from a combination of elemental analysis and TGA analysis. The mass percentages were found to be 4.64% Na/23.4% Ni/41.8% Bi by elemental analysis, which results in mole ratios of 1.01:2.00:1.00 for Na, Ni, and Bi, respectively. To reflect the precision in the experiments, a Na/Ni/Bi ratio of 1:2:1 is employed for the formula. Since hydration occurs on exposure to air with no decomposition, we assume the same 1:2:1 ratio for the anhydrate. TGA reduction, shown in Figure 2A, was performed to determine the oxygen content,[28,29] assuming the structure reduces to Na_2O, Ni metal, and Bi metal. From the mass loss, we determine the compound has 5.66 O per formula unit. Therefore, we assume an oxygen content of 5.66 for data interpretation, i.e., that the formula is $NaNi_2BiO_{5.66}$. TGA analysis was also used to find the water content. As seen in Figure 2B, the anhydrate begins absorbing water nearly immediately on exposure to wet air at room temperature, with water intercalation complete after 24 h. A time-lapsed powder diffraction pattern of the anhydrate on exposure to laboratory air is shown in the inset, though the first peaks indicative of the hydrate are not visible until 4 h after air exposure. The now-hydrated sample can also be dehydrated by heating in the TGA at 0.5 °C/min under air (figure not

dx.doi.org/10.1021/ic501390r | Inorg. Chem. 2014, 53, 10989−10995

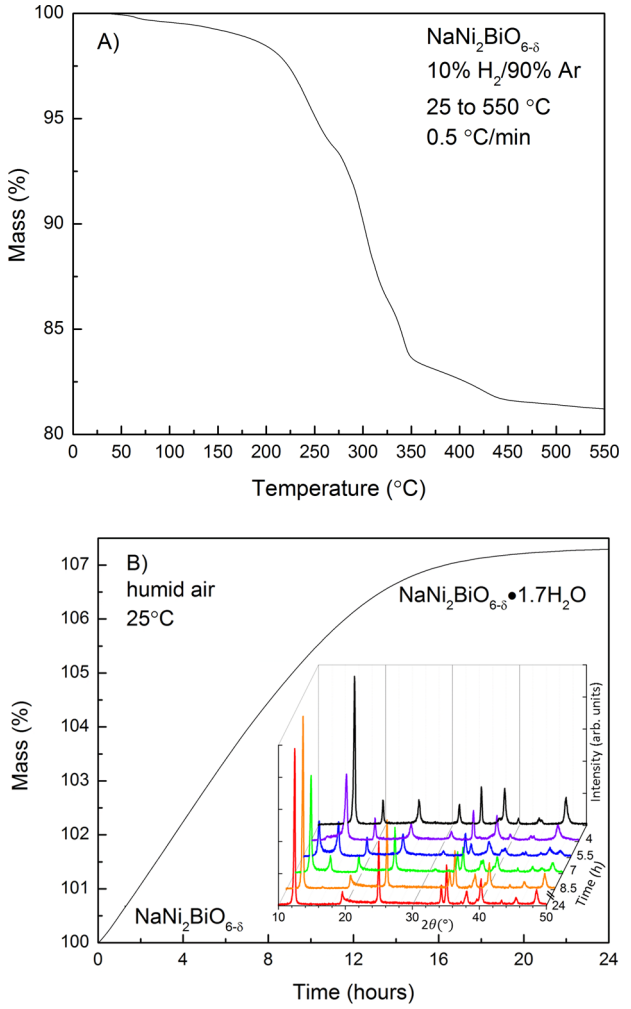

Figure 2. (A) TGA analysis of $NaNi_2BiO_{6-\delta}$ under flowing forming gas (10% H_2, 90% Ar) from 25 to 550 °C at 0.5 °C/min to determine oxygen content. We assume the compound decomposes to Na_2O, Ni, and Bi; mass loss is oxygen loss. (B) TGA analysis showing water uptake of $NaNi_2BiO_{6-\delta}$ to form $NaNi_2BiO_{6-\delta}$·1.7H_2O. Water absorption begins immediately in humid air at room temperature and is complete within 24 h. This water gain amounts to 1.7 H_2O per formula unit. The inset shows the diffraction pattern of the compound over a 24 h period when exposed to ambient laboratory air. The anhydrate is shown in black (back, 0 h), and the hydrate is shown in red (front, 24 h).

shown); both the water uptake and dehydration process via TGA are consistent with 1.7 H_2O per formula unit. The dehydration process yielded a poorly crystallized product that could not be definitively identified, suggesting that water intercalation is not reversible.

Figure 3 shows single crystal precession images of both the anhydrate and hydrate taken at 100 K. Nonsystematic twinning can be observed in both the 0*kl* (panels A and C) and *hk*0 (panels B and D) projections for both compounds. The ordering of the honeycomb layer in both compounds is evident in the *a*−*b* plane. Despite the twinning, the lack of streaking along *c** in the anhydrate indicates that the honeycomb layers do not have stacking faults along *c*; this is markedly different from the parent $Na_3Ni_2BiO_6$ and $NaNi_2BiO_{6-\delta}$·1.7H_2O, where stacking faults appear as streaking along *c** in the 0*kl* projection (panel C).

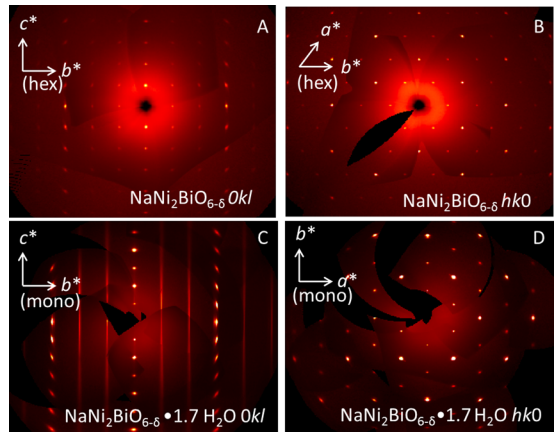

Figure 3. Single crystal precession images of $NaNi_2BiO_{6-\delta}$ (panels A and B) and $NaNi_2BiO_{6-\delta}$·1.7H_2O (panels C and D). No streaking along *c** is observed in the 0*kl* projection of the anhydrate (panel A), whereas significant streaking along *c** is caused by hydration (panel C), indicative of stacking faults. The *a*−*b* plane of both compounds is ordered (panels B and D). The anhydrate indexes to a 1-layer hexagonal cell, whereas the stacking faults in the hydrate prevents a determination of the unit cell.

Structure refinements of the anhydrate single crystal data were challenging due to twinning. By separating the twin domains, $NaNi_2BiO_{6-\delta}$ can be refined in a hexagonal cell with lattice parameters of a = 5.220(3) Å and c = 5.705(5) Å, as shown in Table 1, matching extremely well with powder

Table 1. Single Crystal Structure Determination for $NaNi_2BiO_{6-\delta}$, Experimental Data Taken at 300 K

phase	$NaNi_2BiO_{6-\delta}$
symmetry	hexagonal, *P*-31*m* (No. 162)
cell parameters (Å)	a = 5.220(3), b = 5.220(3), c = 5.705(5)
	$\alpha = \beta$ = 90°; Υ = 120°
wavelength (Å)	Mo Kα, 0.71073
V (Å^3)	134.6(2)
Z	1
calculated density (g cm^{-3})	5.421
formula weight (g mol^{-1})	439.38
absorption coefficient (mm^{-1})	39.5
measured reflections	471
F_{000}	195.0
unique/observed reflections	106/106
data/restraints/parameters	106/0/14
difference e- density (e/Å^3)	+1.25 to −0.823
R_1 (all reflections)	0.0229
wR_2	0.0503
$R_{int}/R(\sigma)$	0.0391/0.0325
GooF	1.108

diffraction measurements. Importantly, the unit cell is therefore a one-layer stacking repeat. The structure must adopt ABAB-type oxygen packing, as ABBA-type packing (the typical 2H-like variants) would cause the octahedra to rotate and require bond-breaking. The analogous Sb-compound, $NaNi_2SbO_6$, was previously made via bromine deintercalation and reported as an R$\bar{3}m$ subcell;[4] it was made more recently by electrochemically cycling $Na_3Ni_2SbO_6$ and was refined as an O1 phase in *P*$\bar{3}$1*m* (no. 162).[30] A fit to *P*$\bar{3}$1*m* also gave the best refinement of our anhydrate single crystal data for $NaNi_2BiO_{6-\delta}$. We draw two main conclusions from our data. First, when the sodium

dx.doi.org/10.1021/ic501390r | *Inorg. Chem.* 2014, 53, 10989−10995

position is allowed to freely refine, it occupies the positions directly below the Ni atoms along z, with no statistically significant density below the Bi atoms (see Table 2 for Wyckoff positions). A model with partial occupancy of the 2d site (1/3, 2/3, 1/2) gives the best fit to the data and suggests that sodium is disordered over these positions between the metal oxide layer and is not present above and below the Bi ions. Sodium sits in octahedral coordination; as such, this is an O1 structure and is an O1 (monoclinic)−O1 (hexagonal) transition from the parent to the anhydrate. Second, the model with the Bi in the center of the octahedron has too much density at the Bi sites, which can be resolved by allowing some of the Bi atoms to move out of the center of the octahedron. This was modeled by creating an "extra" Bi site above and below the in-plane atoms and allowing the Bi density to spread over the two sites. This resulted in approximately 8% of the Bi shifting out of the plane along z. This serves as an indication of motion of the Bi atoms out of plane (allowed by the missing sodium atoms above and below the Bi atoms) which we propose forms a complex defect related to the oxygen vacancies. Because such displacements appear to be randomly distributed, a local structural probe would be required to determine the local defect configuration. On the other hand, the Ni sites appear to be well localized in the plane.

Table 2. $NaNi_2BiO_{6-\delta}$, Space Group P-31m (No. 162)

atom type	label	Wyckoff	x	y	z	S.O.F.
Na	Na1	2d	1/3	2/3	1/2	1
Ni	Ni1	2c	1/3	2/3	0	1
Bi	Bi1	1a	0	0	0	0.919(5)
Bi	Bi2	2e	0	0	0.114(5)	0.040(2)
O	O1	6k	0.353(1)	1.0	0.181(1)	0.943

The occupancies of Na, Ni, and Bi were allowed to freely refine; their occupancies were found to be within 1% of the elemental analysis ratios and were therefore fixed. The oxygen occupancy was fixed to 5.66 based on the TGA analysis. The final structure model is presented in Figure 4, and Table 3 presents selected bond distances. Sodium−oxygen bond lengths are slightly longer than $Na_3Ni_2BiO_6$,[11] consistent with increased 00l layer spacing, and Ni−O and Ni−Ni bond lengths are consistent with Ni oxidation. Note that the symmetry of this space group does not allow for any Jahn−Teller distortion

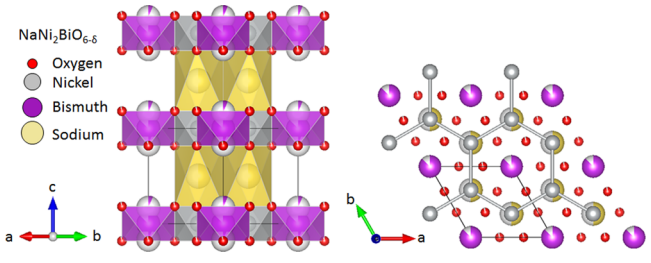

Figure 4. Proposed structure of $NaNi_2BiO_{6-\delta}$. Oxygen is shown in red, nickel in gray, bismuth in purple, and sodium in yellow. Partial occupancies are shown as partially shaded atoms; shading is proportional to occupancy. Note that sodium sites are half-occupied. The left figure illustrates the Bi site splitting, with partial density above and below the honeycomb layer to accommodate the apparent buckling of the Bi atoms. The right figure is a projection of the a−b plane showing the honeycomb packing of the NiO_6/BiO_6 polyhedra. Sodium atoms sit directly below the Ni atoms.

Table 3. $NaNi_2BiO_{6-\delta}$ Selected Bond Distances

atom 1	atom 2	distance, Å
Na1	O1	2.491(8)
Ni1	O1	1.978(6)
Ni1	Ni1	3.014(1)
Bi1	O1	2.106(6)
Bi2	O1	1.878(7)
		2.49(2)

of Ni^{3+}; specification of any local distortion would require further study by a local structure probe. The PXRD data indicates a small (<5%) NiO impurity phase remains in the polycrystalline samples from the parent starting material.

The single crystal data of the hydrate $NaNi_2BiO_{6-\delta}\cdot 1.7H_2O$ could not be refined due to both twinning and the complication of the stacking faults. We index the hydrate to a 1-layer model in $C2/m$ (no. 12) using the powder diffraction data by the Le Bail method, as shown in Figure 5. While other space groups

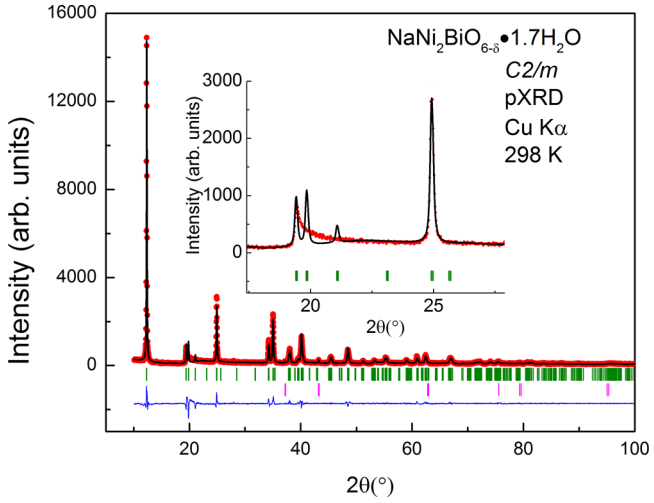

Figure 5. Le Bail fit of the PXRD data for $NaNi_2BiO_{6-\delta}\cdot 1.7H_2O$ in $C2/m$ at room temperature. Observed (red), calculated (black), and difference (blue) plots are shown. The set of green tick marks are Bragg reflections for the respective honeycomb phase; the magenta tick marks are Bragg reflections from a small NiO impurity phase. The inset shows the significant intensity mismatch caused by stacking faults at approximately 20−25° 2θ.

(and number of layers in the unit cell) are possible for this structure, we chose to index this hydrate in $C2/m$ for ease of comparison to its parent structure and to other related compounds in the literature. The presence of the (020) reflection (~20° 2θ) confirms that the integrity of the Ni/Bi ordering is maintained on hydration. Even with the broad warren shape caused by the stacking defects,[21,31] we still find $C2/m$ to give a good qualitative fit to the data and a χ^2 of 4.6 with an NiO impurity phase. The lattice parameters are presented in Table 4, with a and b in agreement with the single crystal data. Quantitative structure refinements of the X-ray powder diffraction data were unable to distinguish individual sodium and water positions due to the stacking faults in the structure and possible disorder within the sodium/water layer. The same issues arise in other MLH materials where, to the authors' knowledge, quantitative structure refinements of sodium MLHs all involve some form of sodium/water disorder in the model or bond distance constraints.[5,9,6,8] Though we

dx.doi.org/10.1021/ic501390r | Inorg. Chem. 2014, 53, 10989−10995

Table 4. $Na_3Ni_2BiO_6$, $NaNi_2BiO_{6-\delta}$, and $NaNi_2BiO_{6-\delta}\cdot 1.7H_2O$ Lattice Parameters

	$Na_3Ni_2BiO_6$[a]	$NaNi_2BiO_{6-\delta}$[b]		$NaNi_2BiO_{6-\delta}\cdot 1.7H_2O$[b]
space group	*C*2/*m*	*P*-31*m*	pseudomonoclinic[c]	*C*2/*m*
a (Å)	5.3998(1)	5.220(3)	5.220	5.2667(1)
b (Å)	9.3518(2)	5.220(3)	9.041	9.1042(3)
c (Å)	5.67997(8)	5.705(5)	5.705	7.3398(2)
β (Å)	108.562(1)	90	90	104.041(4)

[a]Ref 11. [b]This work. [c]$a_{mono} = a_{hex}$; $b_{mono} = (3)^{1/2}(a_{hex})$; $c_{mono} = c_{hex}/(\sin(180 - \beta))$.

cannot determine the coordination of sodium, we can conclude that the oxygen packing sequence must change to a derivative of the three-layer $R\bar{3}m$ subcell. Figure 6 illustrates schematically

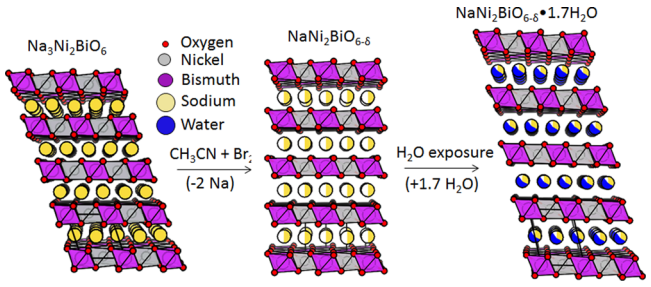

Figure 6. Comparison of $Na_3Ni_2BiO_6$ (left), $NaNi_2BiO_{6-\delta}$ (middle), and $NaNi_2BiO_{6-\delta}\cdot 1.7H_2O$ (right). The removal of sodium and subsequent oxidation of nickel causes layer gliding from a monoclinic to hexagonal structure. Hydration causes layer gliding back to a monoclinic structure. Importantly, the structural transformations occur by layer gliding not by metal-oxide bond breaking. Note that the structure of the anhydrate is simplified, with no buckling of the Bi atoms or oxygen vacancies. The structure of $NaNi_2BiO_{6-\delta}\cdot 1.7H_2O$ is not a refined structure; we show sodium in octahedra with ABCABC packing but it could be another $R\bar{3}m$ subcell variant. Sodium and water are shown disordered on the same site.

the transformation from $Na_3Ni_2BiO_6$ to $NaNi_2BiO_{6-\delta}$ to $NaNi_2BiO_{6-\delta}\cdot 1.7H_2O$. Table 4 gives a comparison of the parent, anhydrate, and hydrate lattice parameters. We show a "pseudo-monoclinic" unit cell for the anhydrate for ease of comparison to the other structures.

Magnetism. The magnetism of $NaNi_2BiO_{6-\delta}$ and $NaNi_2BiO_{6-\delta}\cdot 1.7H_2O$ are both caused by the interactions of nickel ions on the honeycomb lattice. $NaNi_2BiO_{6-\delta}\cdot 1.7H_2O$ (with a layer spacing of ~7.1 Å) represents a quasi 2-D honeycomb, whereas $NaNi_2BiO_{6-\delta}$ is more 3-D in character (with a layer spacing of ~5.7 Å). Both compounds display a subtle magnetic transition at approximately 5 K in the temperature-dependent susceptibility (Figure 7), though it is broader in the hydrate. The nature of this transition may be complex, given that the parent material $Na_3Ni_2BiO_6$ has both AFM and ferromagnetic (FM) magnetic coupling present, as do the honeycomb compounds $Cu_3Co_2SbO_6$ and $Cu_3Ni_2SbO_6$.[11,32] Qualitatively, the magnetic behavior is very similar to that seen in the related hydrate $Na_{0.95}Ni_2SbO_6\cdot 1.5H_2O$.[4] Fitting the high-temperature range (150–300 K) of the anhydrate and hydrate to the Curie–Weiss law ($\chi = C/(T - \theta)$) with small temperature-independent terms ($\chi_o = 3.5 \times 10^{-4}$ for the anhydrate; $\chi_o = -2 \times 10^{-4}$ for the hydrate) yields Weiss temperatures of −18.5(1) K and −14.6(1) K, respectively, indicative of dominantly AFM coupling. The effective moments were found to be 2.26(1) μ_B/Ni and 2.21(1) μ_B/Ni, respectively, which is quite similar to the moment found for $Na_{0.95}Ni_2SbO_6\cdot 1.5H_2O$ (2.28 μ_B/Ni).[4] Both moments are significantly lower than the moment observed for the spin-1 Ni^{2+} parent compound $Na_3Ni_2BiO_6$, (2.81 μ_B/Ni)[11] yet higher than the 1.85 μ_B/Ni observed in the spin-1/2, Ni^{3+} triangular lattice compound $NaNiO_2$.[33] The high moments for the current compounds can be explained either by an unusually high *g* factor or by the presence of a mixture of Ni^{2+} and Ni^{3+} in the compound. Such a mixture could be caused by oxygen vacancies, as evidenced by TGA reduction and the single crystal refinement of the anhydrate. Low-temperature deintercalation reactions (like the bromine treatment used here) of layered ABO_2 compounds are often accompanied by oxygen deficiencies and have been suggested for Na_xCoO_2, $Li_{1-x}CoO_2$ and $Li_{1-x}Ni_{0.5}Mn_{0.5}O_2$.[34,35] If we assume that the nickel atoms are either Ni^{2+} or Ni^{3+} and can be estimated by a *g*-value in the range of 2–2.1, then an effective moment of 2.21 μ_B/Ni (anhydrate) would represent approximately 62%–71% Ni^{3+} and 38%–29% Ni^{2+} and would imply a formula in the range of $NaNi_2BiO_{5.62}$ to $NaNi_2BiO_{5.71}$. Because this range is in close agreement with the oxygen content calculated from TGA data ($NaNi_2BiO_{5.66}$), the compounds studied in this work should be considered as $NaNi_2BiO_{6-\delta}$ and $NaNi_2BiO_{6-\delta}\cdot 1.7H_2O$ with $\delta \approx 0.34$. We estimate the fraction of oxygen vacancies to be ~0.34/6 ≈ 5.6% of the oxygen lattice.

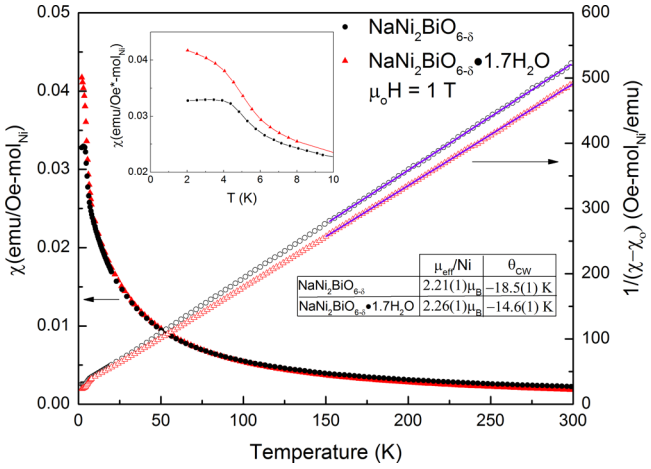

Figure 7. ZFC magnetic susceptibility of $NaNi_2BiO_{6-\delta}$ and $NaNi_2BiO_{6-\delta}\cdot 1.7H_2O$ as a function of temperature from 2 to 300 K in an applied field of 1 T. The black circles correspond to the anhydrate; red triangles are the hydrate. Filled data points are χ as a function of temperature. The upper-left inset displays χ vs T at low temperature to more clearly illustrate the broadening of the magnetic transition around 5 K with hydration. The open data points show the inverse χ vs T with a small correction. The high-temperature data (150–300 K) was fit to the Curie–Weiss law (purple line). The effective moments and Weiss temperatures are summarized in the table.

dx.doi.org/10.1021/ic501390r | Inorg. Chem. 2014, 53, 10989–10995

Field-dependent magnetization of $NaNi_2BiO_{6-\delta}$ and $NaNi_2BiO_{6-\delta}\cdot 1.7H_2O$ taken at 2, 10, and 30 K is shown in Figure 8.

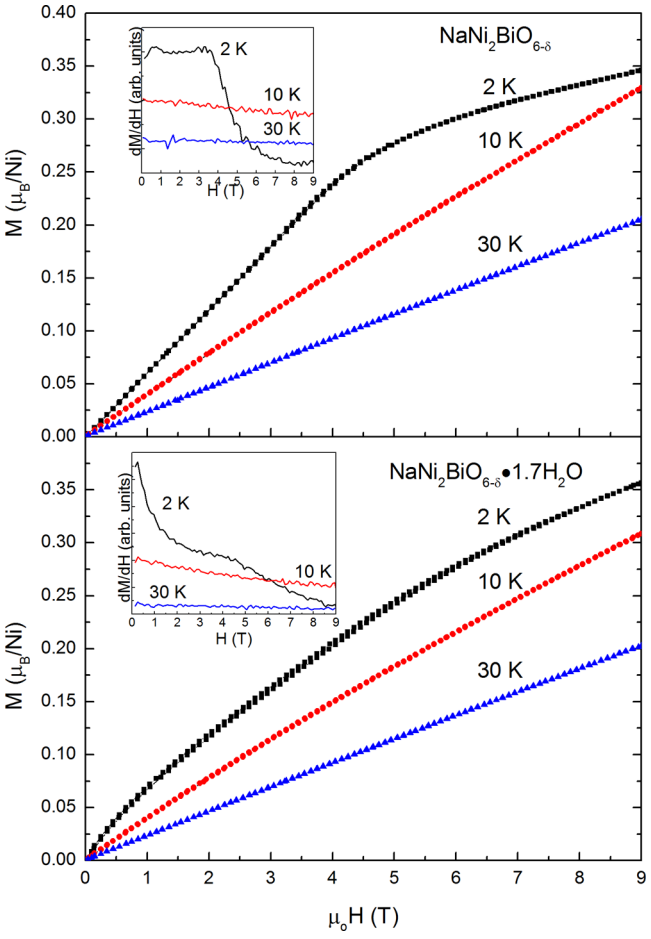

Figure 8. DC-magnetization as a function of applied field for $NaNi_2BiO_{6-\delta}$ (top) and $NaNi_2BiO_{6-\delta}\cdot 1.7H_2O$ (bottom) taken at 2 K (black squares), 10 K (red circles), and 30 K (blue triangles). The anhydrate is linear from zero to approximately 4 T at 2 K. A magnetic transition occurs around 4 T, seen more clearly in the inset (dM/d**H** vs **H**). Slight curvature exists in the 10 K data. For the hydrate, the slope of the 2 K magnetization data is nonlinear and changes at 1 and 4.5 T (dM/d**H** vs **H**, inset), which may indicate subtle magnetic transitions. Similar to the anhydrate, the magnetization is slightly curved at 10 K. Magnetic saturation is not yet reached by 9 T in either compound.

The M vs **H** behavior of the anhydrate is linear at 2 K (below the ordering transition) from 0 to 4 T, above which point a field-induced transition occurs. There may also be a second transition beginning around 8.5 T. On the other hand, we observe curvature in all applied fields in the 2 K data of the hydrate and slight hysteresis. This is unlike the case for a simple ordered antiferromagnet, which would have a linear M vs **H** curve in this applied field range. Further, subtle field-induced transitions are apparent in the 2 K data of the hydrate at 1 and ~4.5 T (see dM/d**H**, inset), similar to those observed in $Na_{0.95}Ni_2SbO_6\cdot 1.5H_2O$.[4] The data at 2 K suggests the presence of an interesting quasi-2D system in the hydrated compound, despite the fact that the ordering temperature and the Curie–Weiss θ are very similar to that of the anhydrate. Even at 10 K, which is above the transition temperature (~5 K) observed in the magnetic susceptibility data, the M vs **H** data for both compounds is slightly nonlinear in the 0–9 T applied field range.

The HC data of $NaNi_2BiO_{6-\delta}$ and $NaNi_2BiO_{6-\delta}\cdot 1.7H_2O$ in $\mu_0\mathbf{H}$ = 0, 3, 6, and 9 T applied fields are shown from 2 to 25 K in Figure 9. No features appear above 25 K. In contrast to the

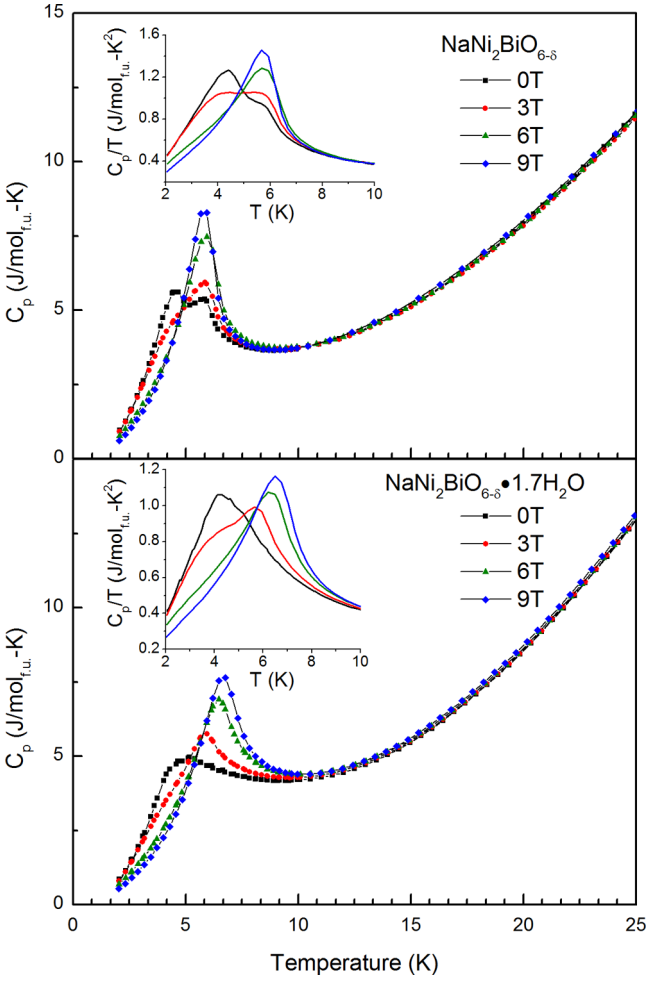

Figure 9. Heat capacity data of $NaNi_2BiO_{6-\delta}$ (top) and $NaNi_2BiO_{6-\delta}\cdot 1.7H_2O$ (bottom) in applied fields of 0 T (black squares), 3 T (red circles), 6 T (green triangles), and 9 T (blue diamonds). $NaNi_2BiO_{6-\delta}$ displays two magnetic transitions at approximately 6.5 and 4 K. The lower temperature transition is suppressed by the applied field, whereas the higher-temperature transition is sharpened. $NaNi_2BiO_{6-\delta}\cdot 1.7H_2O$ has a broad anomaly caused by the magnetic transition beginning around 10 K and reaching a maximum around 6 K. The transition is sharpened and shifts to higher temperature with the application of an external field. The insets show C_p/T vs T.

lambda-like anomaly seen in the zero-field heat capacity data of the $Na_3Ni_2BiO_6$ parent which reaches a maximum of roughly 36.5 $J/mol_{f.u.}$-K at 10.4 K, $NaNi_2BiO_{6-\delta}$ displays two small transitions at 4.5 and 6 K. At 3 T, both transitions are still present, though the 4.5 K transition is diminished; by 6 T, the 4.5 K transition is suppressed and the 6 K transition sharpens into a lambda-like feature. $NaNi_2BiO_{6-\delta}\cdot 1.7H_2O$ has a very broad transition in zero applied field, similar to $NaNi_2SbO_6\cdot 1.5H_2O$, which begins around 10 K and reaches a maximum in the same vicinity as the anhydrate (around 5 K). The application of an external field sharpens this transition and shifts it to higher temperature. The nature of these transitions is unknown at this time, though they are consistent with the

dx.doi.org/10.1021/ic501390r | Inorg. Chem. 2014, 53, 10989–10995

ordering temperatures observed in the magnetic susceptibility. As with the magnetic susceptibility, hydration manifests itself in a broader heat capacity transition.

CONCLUSIONS

The structure and magnetic properties of the Ni^{3+}-based honeycombs $NaNi_2BiO_{6-\delta}$ and $NaNi_2BiO_{6-\delta}\cdot 1.7H_2O$ are presented. A redox reaction of the parent compound removes two Na per formula unit, oxidizing the Ni and causing layer shifting from an ABCABC-type oxygen packing sequence to a 1-layer, ABAB-type packing sequence with hexagonal symmetry. Hydration causes another layer shift back to a three-layer derived structure with an $R\bar{3}m$ subcell. A slight decrease in dimensions of the $a-b$ plane as compared to the parent is caused by the oxidation of Ni^{2+} to Ni^{3+}. Significant expansion of the layer spacing to ∼7.1 Å is observed with hydration. Though $NaNi_2BiO_{6-\delta}$ and $NaNi_2BiO_{6-\delta}\cdot 1.7H_2O$ have similar temperature-dependent magnetic susceptibilities, the transition of the hydrate is much broader; we attribute this to its increased two-dimensionality. Both compounds have a higher-than-expected magnetic moment if all the Ni is 3+ and spin-1/2; this can be explained by an admixture of Ni^{2+}/Ni^{3+} caused by ∼5.6% oxygen vacancies, consistent with TGA data. The magnetization of the hydrate as a function of applied field is nonlinear from 0 to 9 T below the transition temperature, indicating the presence of a magnetic state that is more complex than simple Néel ordering. The anhydrate displays two magnetic transitions in the heat capacity, one which can be suppressed and the other enhanced by an external field, whereas the hydrate has a broad transition that sharpens and shifts with the field. Further investigation, possibly by XANES, would be of interest to further characterize the Ni oxidation state(s), as this is important in interpreting the exact nature of the observed magnetic transitions. Our study demonstrates that the $Na_3Ni_2BiO_6$–$NaNi_2BiO_6$ system has rich magnetic properties which can be tuned by oxidation, H_2O intercalation, and applied magnetic field.

ASSOCIATED CONTENT

Supporting Information

CIF file of $NaNi_2BiO_{6-\delta}$.This material is available free of charge via the Internet at http://pubs.acs.org.

AUTHOR INFORMATION

Corresponding Authors

*E-mail: eseibel@princeton.edu.
*E-mail: rcava@princeton.edu.

Notes

The authors declare no competing financial interest.

ACKNOWLEDGMENTS

This work was supported by the DOE through the Institute for Quantum Matter at Johns Hopkins University, Grant DEFG02-08ER45644. The authors would like to thank Girija Sahasrabudhe and Dr. Rob L'Esperance for helpful discussions.

REFERENCES

(1) Regnault, L. P.; Rossat-Mignod, J. Phase Transitions in Quasi Two-Dimensional Planar Magnets. In *Magnetic Properties of Layered Transition Metal Compounds*; De Jongh, L., Ed.; Kluwer Academic Publishers: Dordrecht, The Netherlands, 1989; pp 271–321.
(2) Chaloupka, J.; Jackeli, G.; Khaliullin, G. *Phys. Rev. Lett.* **2010**, *105*, 027204(1)–027204(4).
(3) Anderson, P. W. *Science* **1987**, *235*, 1196–1198.
(4) Roudebush, J. H.; Cava, R. J. *J. Solid State Chem.* **2013**, *204*, 178–185.
(5) Takada, K.; Sakurai, H.; Takayama-Muromachi, E.; Izumi, F.; Dilanian, R. A.; Sasaki, T. *J. Solid State Chem.* **2004**, *177*, 372–376.
(6) Park, S.; Yoon, W. S.; Vogt, T. *Solid State Commun.* **2007**, *142*, 75–79.
(7) Park, S.; Lee, Y.; Si, W.; Vogt, T. *Solid State Commun.* **2005**, *134*, 607–611.
(8) Park, S.; Kang, K.; Si, W.; Yoon, W. S.; Lee, Y.; Moodenbaugh, A. R.; Lewis, L. H.; Vogt, T. *Solid State Commun.* **2005**, *135*, 51–56.
(9) Shikano, M.; Delmas, C.; Darriet, J. *Inorg. Chem.* **2004**, *43*, 1214–1216.
(10) Park, S.; Lee, Y.; Elcombe, M.; Vogt, T. *Inorg. Chem.* **2006**, *45*, 3490–3492.
(11) Seibel, E. M.; Roudebush, J. H.; Wu, H.; Huang, Q.; Ali, M. N.; Ji, H.; Cava, R. J. *Inorg. Chem.* **2013**, *52*, 13065–13611.
(12) Rodriguez-Carvajal, J. *J. Phys. B* **1993**, *192*, 55–69.
(13) *APEX II*; Bruker AXS Inc: Madison, Wisconsin, USA, 2013.
(14) *CELL_NOW*; Bruker AXS Inc.: Madison, Wisconsin, USA, 2013.
(15) *SHELXTL*; Bruker AXS Inc.: Madison, Wisconsin, USA, 2013.
(16) Farrugia, L. J. *J. Appl. Crystallogr.* **2012**, *45*, 849–854.
(17) Viciu, L.; Bos, J. W. G.; Zandbergen, H. W.; Huang, Q.; Foo, M. L.; Ishiwata, S.; Ramirez, A. P.; Lee, M.; Ong, N. P.; Cava, R. J. *Phys. Rev. B* **2006**, *73*, 174101(1)–174101(10).
(18) Takada, K.; Sakurai, H.; Takayama-Muromachi, E.; Izumi, F.; Dilanian, R. A.; Sasaki, T. *Nature* **2003**, *422*, 53–55.
(19) Breger, J.; Jiang, M.; Dupre, N.; Meng, Y. S.; Shao-Horn, Y.; Ceder, G.; Grey, C. P. *J. Solid State Chem.* **2005**, *178*, 2575–2585.
(20) Smirnova, O. A.; Nalbandyan, V. B.; Petrenko, A. A.; Avdeev, M. *J. Solid State Chem.* **2005**, *178*, 1165–1170.
(21) Politaev, V. V.; Nalbandyan, V. B.; Petrenko, A. A.; Shukaev, I. L.; Volotchaev, V. A.; Medvedev, B. S. *J. Solid State Chem.* **2010**, *183*, 684–691.
(22) Berthelot, R.; Schmidt, W.; Muir, S.; Eilertsen, J.; Etienne, L.; Sleight, A. W.; Subramanian, M. A. *Inorg. Chem.* **2012**, *51*, 5377–5385.
(23) Zvereva, E. A.; Evstigneeva, M. A.; Nalbandyan, V. B.; Savelieva, O. A.; Ibragimov, S. A.; Volkova, O. S.; Medvedeva, L. I.; Vasiliev, A. N.; Klingeler, R.; Buechner, B. *Dalton Trans.* **2012**, *41*, 572–580.
(24) Greaves, C.; Katib, S. M. A. *Mater. Res. Bull.* **1990**, *25*, 1175–1182.
(25) Paulsen, J. M.; Donaberger, R. A.; Dahn, J. R. *Chem. Mater.* **2000**, *12*, 2257–2267.
(26) Berthelot, R.; Pollet, M.; Doumerc, J. P.; Delmas, C. *Inorg. Chem.* **2011**, *50*, 4529–4536.
(27) Kubota, K.; Yabuuchi, N.; Yoshida, H.; Dahbi, M.; Komaba, S. *Mater. Res. Bull.* **2014**, *39*, 416–422.
(28) Cava, R. J.; Zandbergen, H. W.; Ramirez, A. P.; Takagi, H.; Chen, C. T.; Krajewski, J. J.; Peck, W. F.; Waszczak, J. V.; Meigs, G.; Roth, R. S.; Schneemeyer, L. F. *J. Solid State Chem.* **1993**, *104*, 437–452.
(29) Pasero, D.; Reeves, N.; Gillie, L. J.; West, A. R. *J. Power Sources* **2007**, *174*, 1078–1081.
(30) Yuan, D.; Liang, X.; Wu, L.; Cao, Y.; Ai, X.; Feng, J.; Yang, H. *Adv. Mater.* **2014**, *26*, 6301–6306.
(31) Warren, B. E. *Phys. Rev.* **1941**, *59*, 693–698.
(32) Roudebush, J. H.; Andersen, N. H.; Ramlau, R.; Garlea, V. O.; Toft-Petersen, R.; Norby, P.; Schneider, R.; Hay, J. N.; Cava, R. J. *Inorg. Chem.* **2013**, *52*, 6083–6095.
(33) Chappel, E.; Nunez-Regueiro, M. D.; Dupont, F.; Chouteau, G.; Darie, C.; Sulpice, A. *Eur. Phys. J. B* **2000**, *17*, 609–614.
(34) Banobre-Lopez, M.; Rivadulla, F.; Caudillo, R.; Lopez-Quintela, M. A.; Rivas, J.; Goodenough, J. B. *Chem. Mater.* **2005**, *17*, 1965–1968.
(35) Venkatraman, S.; Manthiram, A. *Chem. Mater.* **2003**, *15*, 5003–5009.